Journal of Scientific Research
Banaras Hindu University, Varanasi

Vol. 62, 2018 : 171-202
ISSN : 0447-9483

STATUS OF DARK MATTER SEARCH

M.K. Singh[1], V. Sharma[1.2], M.K. Singh[1.2], K. Saraswat[1], D. Grover[1], A. Kumar[1], N. Marimuthu[1], A Pandey[1], P. Kumar[1], V. Singh*[1] and Henry Tsz-king Wong[2]

1. Department of Physics, Institute of Science, Banaras Hindu University, Varanasi-221005, India.
2. Institute of Physics, Academia, Sinica, Taipei, 11524 Taiwan, *Email: venkaz@yahoo.com

Abstract

Dark matter is among the most important and long standing open problems in modern physics. Contrary to our understanding, it is observed that the orbital velocity of a star in a galaxy increases with distance away from the center. It means there is more mass in the galaxy than the luminous mass. Dark matter is postulated by Jan Oort in 1932 to account for this effect. There are also observations that the distant galaxies are moving faster as time proceeds. There is constant energy density of the space which does not dilute with the expansion and is referred as Dark Energy. On the basis of all the observations and model calculations the composition of the universe is understood to be only ~4 % visible matter, ~70% dark energy and ~26 % dark matter. Various dark matter candidates have been proposed by several models in the support of the presence of dark matter but till date dark matter candidate is not yet discovered. The Weakly Interacting Massive Particles (WIMPS) are the most accepted candidates for dark matter. We used Germanium ionization detectors, which can be capable of observing rare weakly interacting particles by discriminating them from all known type of background particles and radiations including low energy neutrons. The goal is also to achieve very low detection threshold to observe dark matter candidate WIMP such as neutralinos. A large array of this type of detector will have discovery potential for the Dark Matter and can also be used to measure properties of neutrino from reactors or from the supernova. The detector has simple detection principle requiring limited electronics and also portable. It can also be used for the detection of neutrinoless double beta decay searches. Germanium ionization detectors are novel techniques offering kg-scale radiation sensors with sub-keV sensitivities. Germanium ionization detectors have been used for the studies of neutrino interactions and properties as well as to search for light WIMP Dark Matter. However, anomalous surface behavior, which needs to be characterized and understood. Crucial to this study, is the understanding of the selection procedures for the bulk and surface events differentiation in the sub-keV range of energy. In this report we will describe the detector characterization methods and results which are used to identify the bulk and surface events in the analysis techniques. In addition, the atomic effects due to neutrino electromagnetic properties were derived, and constraints were placed with reactor neutrino data, are summarized.

Keywords: WIMP Dark matter candidate searches, Neutrino magnetic moment, Germanium ionization detector, Surface & Bulk events.

Introduction

In astronomy and cosmology, dark matter is matter that is inferred to exist from gravitational effects on visible matter and background radiation, but is undetectable by

emitted or scattered electromagnetic radiation. The Universe has more mass in the galaxy than the luminous mass.

Historically, three categories of dark matter candidates had been postulated; ***cold dark matter*** – particles that move at classical velocities, ***hot dark matter*** – particles that have relativistic velocity, and ***warm dark matter.*** "Cold" dark matter is dark matter composed of constituents with a free-streaming length much smaller than the ancestor of a galaxy-scale perturbation. This is currently the area of greatest interest for dark matter research, as hot dark matter does not seem to be viable for galaxy and galaxy cluster formation. Weakly Interacting Massive Particles (WIMPs) are the most accepted candidates of cold dark matter by theoretical models.

The dark matter search experiments are divided into two classes: ***direct detection experiments***, which search for the scattering of dark matter particles off atomic nuclei within a detector; and ***indirect detection***, which look for the products of WIMP annihilation or decay.

1.1 Indirect Detection Experiments

Indirect detection experiments search for the products of WIMPs annihilation. If WIMPs are Majorana particles, the particle and antiparticle are the same, and then two WIMPs colliding would annihilate to produce gamma rays, and particle-antiparticle pairs. Additionally, if the WIMP is unstable, WIMPs could decay into standard model particles. These processes could be detected indirectly through an excess of gamma rays, antiprotons or positrons emanating from regions of high dark matter density. The detection of such a signal is not conclusive evidence for dark matter, as the production of gamma rays from other sources is not fully understood. The EGRET gamma ray telescope observed more gamma rays than expected from the Milky Way, but scientists concluded that this was most likely due to a wrong estimation of the telescope's sensitivity.

1.2 Direct Detection Experiments

Direct detection experiments typically operate in deep underground laboratories to reduce the background from cosmic rays. These include: the Soudan mine; the SNO underground laboratory at Sudbury (Canada); the Gran Sasso National Laboratory (Italy); the Boulby Underground Laboratory (UK); and the Deep Underground Science and Engineering Laboratory, South Dakota (USA) etc. The majority of present experiments use one of the two detector technologies: Cryogenic detectors, operating at temperatures below 100 *mK*, detect the heat produced when a particle hits an atom in a crystal absorber such as germanium and Noble liquid detectors, detect the flash of scintillation light produced by a particle collision in liquid Xenon or Argon. Both of these detector types are capable of distinguishing background particles which scatter off electrons from dark matter particles which scatter off nuclei. Cryogenic detector experiments include: CDMS, CRESST, EDELWEISS, EURECA, CoGent, TEXONO,

PICASSO and CDEX. Noble liquid experiments include ZEPLIN, XENON, DEAP, ArDM, WARP and LUX.

1.3 Importance of Direct Detection

Direct DM search is based on the detection of nuclear recoils induced by WIMP scattering. WIMP (mass 10-1000 GeV) having low speed, interacts with ordinary matter via elastic scattering on nuclei, which results in that the typical recoil energy between 1 and 100 keV. The average energy of recoils significantly increases as the WIMP mass gets larger. The motion of the Earth around the Sun induces a time modulation of the expected flux of WIMP with an annual period. The motion of the Sun inside the galaxy also causes anisotropy in the nuclear recoils induced by WIMPs. The time modulation and anisotropy of detected nuclear recoils are the clear evidences for a WIMP signal in direct search experiments.

Assuming a smooth distribution of WIMPs, the flux is peaked in the direction opposite to the motion of the Sun in the galaxy, so the Earth must "see" an apparent WIMP wind. The angular distribution of nuclear recoils has to show a peak in this direction. For a detector based on the Earth, the WIMP wind will appear to come from the Cygnus constellation, this direction changes with a sidereal day period. The evidence of a clear anisotropy in the nuclear recoil distribution, which has never been observed, would unambiguously prove the existence of WIMP particles as DM constituents.

1.4 TEXONO Experiment

Now-a-days, semiconductor ionization detectors technologies have matured for a wide spectrum of applications as radiation detectors. These radiation detectors using germanium crystal sensors are widely in use of experimental nuclear and Astroparticle physics. They provide excellent energy resolution as well as strong absorption to γ – rays and can be fabricated to a large modular mass of the kilogram range. Therefore, they are ideal tools for γ – ray spectroscopy of energy up to 10 MeV range. The themes of the research programs of TEXONO (Taiwan EXperiment On NeutrinO) Collaboration which was established in 1997, are on the studies of low energy neutrino physics such as neutrino nucleus coherent scattering (NNCS), neutrino millicharge, charge radius, neutrino magnetic moments etc. and WIMP dark matter search. To study the low energy neutrino properties and interactions, the collaboration required an intense source of neutrinos. For that, at the Kuo-Sheng Nuclear Power Plant on the Northern Shore of Taiwan, the Kuo-Sheng Reactor Neutrino Laboratory (KSNL) was established in the year 2000 in the vicinity of nuclear reactor No. 1. It is situated on the first floor of the seven-storey reactor building ~12 m below sea level. The standard operation of the Kuo-Sheng Power Plant includes about 18 months of Reactor ON period and about 50 days of Reactor OFF period. Reactor operation data on the thermal power output and control rod status as functions of time and locations within the core are provided, when necessary, to the experiment by the Power Station. The $\bar{\upsilon}_e$[9] s

emitted in power reactors are predominantly produced through β - decays as, (I) Fission products, following the fission of the four dominant fissile isotopes: ^{235}U, ^{238}U, ^{239}Pu and ^{241}Pu, and (II) ^{239}U, following the neutron capture on the ^{238}U fuel: ^{238}U(n), ^{239}U. The $\bar{\upsilon}_e$ production rate at KSNL is 6.4×10^{12} cm^{-2} sec^{-1}.

This manuscript is divided in four sections. Second section explains the physics goals of the TEXONO experiment. Section third described the experimental facilities of TEXONO, various sub-keV Germanium detectors used in TEXONO for different physics goals [3], bulk / surface event differentiation techniques in sub-keV region [5]. Section four described the achievements of TEXONO experiment in Dark Matter search [14] Neutrino physics [10, 11, 20] as well as the current status and future goals.

2. Physics Motivations of TEXONO Experiment

Semiconductor detectors have found broad range of applications during recent decades, in particular for gamma and soft X-ray spectrometry and as particle detectors. Germanium detectors with sub–keV sensitivities have been demonstrated as efficient means to probe Weakly Interacting Massive Particles [1–3] – a strongly motivated and model supported dark matter candidate. This novel detector technique is also adopted in the studies of neutrino – nucleus coherent scattering with reactor neutrinos [4]. This motivated the development of p-type point – contact germanium detectors (pGe). The advantages of point contact germanium detector are described in sec. 3.1.1. The experimental signatures of such scattering/interactions are the nuclear recoils, posing the challenging requirements of low background and low threshold to the detectors. For the proof of principle a small mass detector are good enough but for the discovery purpose experiments requires large mass detectors. As we know that the background inside the detector is proportional to the detector's mass and the present technology of germanium crystal growth imposes limitations on the size of the germanium crystal and also on the mass. That's the reason almost all germanium based experiments that are either searching for neutrinoless double beta decay or neutrino-nucleus coherent scattering cross section or searching for dark matter candidates, are using a ~kg mass germanium detector in array form and planning to reach up to tons scale detector. We exploit the germanium detector technology to achieve world's lowest detection threshold. The theme is to explore high–purity germanium (HPGe) detector technology to develop a sub–keV threshold detector for pursuing studies on low energy neutrino and dark matter physics. On the way of detector development, we encounter that the surface and bulk events features in the pGe detector exhibit anomalous behavior [5], although surface events are almost absent in case of nGe detector. TEXONO Collaboration has developed and used several HPGe detectors, the largest of which are point–contact germanium detectors of modular mass of 1 kg [3]. The generic benchmark goals in terms of detector performance for the above mentioned physics objectives are: (i) modular target mass of order of 1 kg; (ii) detector sensitivities reaching the range of 100 eV; (iii) background at the range of 1 count kg^{-1}keV^{-1}day^{-1} (cpkkd).

2.1 Neutrino electromagnetic properties

The studies on possible neutrino electromagnetic interactions [6] can probe physics beyond the Standard Model. Neutrino magnetic moment (μ_υ) is an intrinsic neutrino property that describes possible neutrino–photon couplings via its spin [7, 8]. The helicity is flipped in μ_υ induced interactions. Observations of μ_υ at levels relevant to present or future generations of experiments strongly favor the neutrinos as Majorana particles [9]. As shown in Figure 1(a), the μ_υ contributions are enhanced as T decreases, with modifications of the atomic binding energy effects [10] here; T denotes the recoil energy of electron. In a similar way, studies of neutrino millicharge (δ_Q) probe possible helicity–conserving QED–like interactions. Finiteness of δ_Q would imply that neutrinos are Dirac particles. It was recently recognized that there is enhancement in cross–sections due to atomic effects [11], as depicted in Figure 1(a). The known ratios of the peaks and discrete binding energies provide smoking gun signatures for positive observations.

2.2 Neutrino - nucleus coherent scattering

Neutrino coherent scattering with the nucleus (υ_N) [1, 4], $\nu + N \rightarrow \nu + N$, is a fundamental neutrino interaction which has never been observed. Measurement of υ_N coherent scattering would provide a sensitive test to the Standard Model. The coherent interaction plays an important role in astrophysical processes. Coherent neutrino scattering may provide new approaches towards the detection of supernova neutrinos and offer a promising avenue towards a compact and relatively transportable neutrino detector for real–time monitoring of nuclear reactors operation. The maximum nuclear recoil energy for Ge target (A = 72.6) due to reactor $\bar{\upsilon}_e$ is about 2 keV. The quenching factor is about 20% for Ge in the region of below 10 keV. Accordingly, the maximum measurable energy is about 400-500 eV [3]. The typical differential spectrum and the integral event rate as a function of physics threshold are given in Figures 1 (a&b), respectively. At the benchmark sensitivities, the expected rate is of the order of 10 $kg^{-1}day^{-1}$ with signal to background ratio > 50 at a threshold of 100 eV has been achieved. Therefore, low detector threshold is crucial in such experiments.

2.3 WIMP Dark Matter Searches

About one–quarter of the energy density of the universe can be attributed to cold dark matter [12] whose nature and properties are unknown. Weakly Interacting Massive Particles (WIMPs denoted by χ) are its leading candidates. The WIMPs interact with matter pre-dominantly via the same coherent scattering mechanism like the neutrinos: $\chi + N \rightarrow \chi + N$There may be both spin-independent and spin-dependent interactions between WIMP and matter. Most experimental programs optimize their design in the high–mass region and exhibit diminishing sensitivities for m_χ<10 GeV. To probe the low–mass WIMPs region, detector with sub–keV threshold is necessary. Such threshold presents a formidable challenge to detector technology and for background control. The nuclear recoil spectra at $10^{-40}cm^2$ for several WIMP mass (m_χ)

for Ge are displayed in Figure 1 (a). Therefore, the advantages of having a low threshold detector are as follows:

(I) A reduction in detector threshold opens a new window for observation of WIMPs with lower masses. The sensitivity reach on m_χ with 1 kg–yr of exposure as a function of threshold at a background of 1 $kg^{-1}keV^{-1}day^{-1}$ is illustrated in the inset of Figure 2(a).

(II) The low threshold allows a larger range of WIMPs to contribute in an observable interaction and hence results in better sensitivities for all values of m_χ, as illustrated in the Figure 2(b).

3. Experimental details

The Kuo-Sheng Reactor Neutrino Laboratory is located at distance of 28 m from the core No. 1 and around 102 m from the second nuclear reactor of the Kuo-Sheng Nuclear Power Station operated by the Taiwan Power Company on the northern shore of Taiwan. The nuclear power station has twin nuclear reactors. The nominal thermal power output of each one is 2.9 GW. A schematic view of the nuclear reactor number 1 is depicted in Figure 3(a).

A multipurpose inner target detector space of dimension 100 cm × 80 cm × 75 cm is enclosed by 4π passive shielding materials which have a total weight of about 50 ton. The nominal overburden above the Kuo-Sheng Reactor Neutrino Laboratory is around 30 meter-water-equivalents (mwe). The shielding provides attenuation to the ambient neutron and gamma background, and consists of, from inside out, 5 cm of Oxygen Free High Conductivity (OFHC) copper, 25 cm of boron–loaded polyethylene, 5 cm of stainless steel to support the structure, 15 cm of lead to attenuate the gamma rays, and plastic scintillator panels to veto the cosmic – rays [3]. The schematic layout of the shielding structure is shown in Figure 3(b). In the inner target space, various detectors can be placed for the different scientific programs, simultaneously, on the movable platform.

At the experimental sites the germanium detector – a target detector was enclosed by an NaI(Tl) crystal scintillator detector – as an anti–Compton (AC) detector and copper passive shielding inside a plastic bag purged by nitrogen gas evaporated from the liquid nitrogen Dewar. This setup, shown in Figure 4, was put inside the passive shielding house as shown in Figure 3(b). This whole structure was surrounded by cosmic–ray (CR) veto panels made of plastic scintillator read out by photomultiplier tubes (PMTs) [3]. The NaI(Tl) detector named wall detector provides three side coverage to the target detector. A base detector made up of NaI(Tl) and readout by PMT provides a coverage to the target detector from bottom side.

3.1 Sub-keV threshold Ge detectors

The germanium detector is also called high – purity germanium detector (HPGe) or hyper pure germanium detector. Before advanced purification techniques were

developed, germanium crystals could not be produced with purity sufficient to enable their use as spectroscopy detectors. Impurities in the crystals trap electrons and holes, and ruin the performance of the detectors. Consequently, germanium crystals were doped with lithium ions (Ge(Li)), in order to produce an intrinsic region in which the electrons and holes would be able to reach the contacts and produce a signal. The HPGe detectors commonly use lithium diffusion technique to make an n^+ Ohmic contact, and boron implantation technique to make a p^+ contact. Coaxial detectors with a central n^+ contact are referred to as n – type detectors, while p – type detectors have a p^+ central contact. The thickness of these contacts represents a dead layer around the surface of the crystal within which energy depositions do not result in detector signals. The central contact in these detectors is opposite (in polarity) to the surface contact, making the dead layer in n – type detectors smaller than the dead layer in p – type detectors. Typical dead layer thicknesses are around 0.5 mm for a Li diffusion layer, and around 0.3 micrometer for a B implantation layer. TEXONO collaboration has studied various custom designed and commercially constructed Ge detectors. The Ge detector is used as an ionization detector. In semiconductor detectors, ionizing radiation is measured by the number of charge carriers set free in the detector material which are produced between two electrodes, by the radiation. Under reverse bias, an electric field extends across the intrinsic or depleted region. Ionizing radiation produces free electrons and holes. The germanium has a net impurity level of around 10^{10} atoms/cc so that with moderate reverse bias, the entire volume between the electrodes is depleted, and an electric field extends across this active region. The number of electron–hole pairs is proportional to the energy of the radiation to the semiconductor. As a result, a number of electrons are transferred from the valence band to the conduction band, and an equal number of holes are created in the valence band. Under the influence of an electric field, electrons and holes travel to the electrodes, where they result in a pulse that can be measured in an outer circuit. The holes travel in the opposite direction and can also be measured. As the amount of energy required to create an electron–hole pair is known, and is independent of the energy of the incident radiation, measuring the number of electron-hole pairs allows the intensity of the incident radiation to be determined. The four types of detector configurations used [3] are listed below with their corresponding sensor schematics depicted in Figure 5 for their various physics objectives.

(I) a coaxial p–type high purity Ge detector of 1 kg mass used as target detector in Ref. [8],

(II) n-type ULE–HP Ge detector array having 4 crystals each of mass 5g used as target detector in Refs. [13, 15],

(III) Two p–type point-contact Ge detector (pGe) of mass 900 g and 500 g used as target detector in Refs. [14, 15, 3], and

(IV) n–type point – contact Ge detector (nGe) of mass 500 g used for calibration in Refs. [14, 5].

The High Purity and Ultra Low Energy standard germaniums are conventional technologies. The concept of point-contact Ge detectors was proposed and the first nGe at 800 g mass was constructed in the 1980 [16], followed by recent realization of pGe [2]. The ULEGe, pGe and nGe are of sub–keV sensitivities and with typically less than a pF capacitance. A summary of the detector performance is given in Table 1.

3.1.1 Advances of Point contact over Co-axial germanium detector

Study of experimental rare physics events requires very low background i.e., almost zero background, as low as possible detection threshold, as large as possible detector size and as close as possible placement of detector to the source. To increase the flux of incident particle the last criteria are essential. Rare physics events have extremely low interaction cross section with in detector material and their final signal energy is also very low. In most of the detectors such low energy signals belong to the noise edge region. Commonly used germanium detector in the laboratories is co-axial germanium detector having mass range from few grams to a kilogram. Such detectors have internal capacitance of the order of pF and due to which leakage current value is of the order of few mA. That gives rise to increasing detection thresholds of the detector. If any weakly interacting particle interacts with the detector once it will not interact again in general in the same volume due to very weak interaction cross section. In case of co-axial detector as shown in Figure 5(a), if any particle interacts more than once inside the fiducial volume of this detector will give similar pulse shape as single interaction pulse shape because the drift distance between central electrode and the interaction point are almost same and due to this reason the drift time – time taken by the change to reach the electrode, is also the same. As a result, the pulse shape of multi-sited or multi-interaction events and single-sited event have no difference. But in the case of point contact germanium detector, the central electrode area becomes point shape of dimension of a few mm radius. It makes the internal capacitance of the whole detector less than a pF. As a result the value of leakage current decreases and therefore detection threshold also becomes lower than that of the co-axial detector. The related parameters of the co-axial (1000g) and pGe (900g) detectors are listed in Table 1. From Table 1, one can see that the pedestal noise root mean square has drastic change from 812 eV in case of co-axial detector to 56 eV and in the case of point contact germanium detector. At 50% trigger efficiency the threshold is 3500 eV and 230 eV were obtained for co-axial and point contact germanium detectors, respectively. Due to the point shape of the central electrode of germanium detector as shown in Figure 5 (c & d), the drift distance becomes effective in case of multiple sited events and single sited events and this difference is reflected in the arrival timing of the charge to the electrode. Therefore the shapes of the multi-sited and single-sited events are effectively different and using pulse shape differentiation techniques both type of events may be separated with few percent of overlap. Due to these excellent properties of point contact germanium detector, we observed better energy resolution of such detector than the co-axial detector. The hole – barrier and electron – barrier contacts for point contact germanium detectors are generally fabricated by using Li diffusion and Boron implant

(anneal). There are other options for making contacts such as Ni, Cr, Pt, Pd, Au etc. The usual thickness of Lithium diffused outer contact is ~ 1 mm for co-axial and p+ point contact germanium detector. This thickness usually creates 7-8% Li dead layer of the detector. That results in a loss of valuable ^{76}Ge material as a result increasing the cost of such detector. Thick lithium diffused dead layer causes spectral artifacts in the observed spectrum and also show slow rise time of the pulses from a transition layer.

3.2 Physics event selection

The output of the germanium detector is fed to the input of the preamplifier. The RESETs window opens for few seconds to capture the detailed activity before and after the event, the typical output of the preamplifier as observed in an oscilloscope is displayed in Figure 6(a). The saw–tooth type characteristics exemplify the timing structures of the RESETs which are issued after a fixed time interval or when the charge depositions in the detectors exceed a certain preset value. The steps in between the RESETs represent physics signals with heights proportional to their energy. The preamplifier signals are further processed by shaping and timing amplifiers. A typical shaping amplifier (SA) output pulse is shown in Figure 6(b). The waveform is characterized by several parameters and some of them are shown in Figure 6(b). The noise events are then eliminated by studying the various correlations between the stored waveform parameters. For example, event timing correlated with preamplifier reset signal and distribution of pedestal is shown in Figure 7(a) and 7(b), respectively. The fast–timing, slow shaping, and anti–Compton – NaI(Tl), output were digitized by flash analog–to–digital converters at 200 MHz, 60 MHz and 20 MHz, respectively [3]. The discriminator and timing outputs of the Cosmic–Ray (CR) panels were also recorded. The energy calibration was performed by using X-rays from $^{68,\ 71}$Ge (10.37 keV), ^{65}Zn (8.98 keV) and ^{68,71}Ge + ^{65}Zn (1.29 keV) with random trigger events providing zero-energy definition [3]. As we know that the neutrino and dark matter candidates are weekly interacting with the detector material, therefore the nuclear recoil χ_N and υ_N events are uncorrelated with the rest of the surrounding detector components and are uniformly distributed in point contact germanium detector (pGe) volume and the background that may be physics events, must be correlated with any other detectors. It means we are looking for events having only single sited interaction and uniform distribution in the pGe detector volume. The superscript (–) / (+) denotes (uncorrelated)/(correlated) cosmic – ray (CR) and anti–Compton veto (AC) systems with pGe signals. The $AC^{+}\otimes CR^{-}$ represent an event having hits in anti-Compton veto system and in pGe detector but no hit in cosmic ray veto system. It means that this event belongs to the ambient gamma ray. The $AC^{-}\otimes CR^{+}$ represent an event having hits in cosmic ray veto system and in pGe detector but no hit in anti-Compton veto system. It means that this event belongs to the cosmic ray induced high energy neutron event. The desired signal which is used for further physics study is designated by $AC^{-}\otimes CR^{-}$ having signal only in the target pGe detector. The $AC^{+}\otimes CR^{+}$ represent events having hits in cosmic ray veto and in anti-Compton veto systems along with the pGe detector

are physics events. These events are shown in Figure 7(a) with black and blue colors and the red color mesh is representing noise that has been rejected. Correlation has been established on the basis of fluctuation of pedestal as shown in Figure 7(b), where event pedestal value in keV per electron equivalent (keV_{ee}) is plotted with respect to nuclear recoil energy in keV_{nr}. The random events are NIM signals generated one every 10 seconds, give the information about the zero point on the energy scale and events not belonging to the horizontal band are noise events and have been rejected. In almost all the bands events are the lone events ($AC^{-}\otimes CR^{-}$) showing Ga X-ray peak at 10.37 keV_{ee}.

3.3 Differentiation of bulk and surface events

We observed surface events only in pGe detector. The outer surface electrode of the p–type point contact germanium detector (pGe) is fabricated by lithium diffusion technique, giving a finite thickness. In principle, there is no electric field within the undepleted surface layer of the detector to influence the trajectory of charge, so electrons and holes within this region move only due to diffusion. Charges are deposited by the radiation at varying distances from the detector's surface diffuses, and the fraction of the total charge that reaches the boundary between the surface layer and the depleted region of the detector is recorded by the DAQ at very fine time intervals of the order of nanoseconds. It can take many microseconds for holes created in the surface layer to reach the bulk of the detector and induce a signal on the electrode, resulting in charge signals that take several microseconds to reach their maximum value. This is in sharp contrast to events that occur in the bulk, where all holes are collected through the high field region in several hundred nanoseconds. In practice, electron–hole pairs produced by radiations at the surface layer are subjected to a weaker drift field than those inside the crystal bulk region. The surface–events have only partial charge collection and slower rise–time [3, 5, 14]. The difference in the event rise–time, i.e., the time it takes for the charge signal to reach its maximum value, can be used to distinguish bulk events from surface events and, ultimately, remove surface events from the data set for further analysis. The thickness of the surface layer was derived to be (1.16 ± 0.09) mm, via the comparison of simulated and observed intensity ratios of γ – peaks from a ^{133}Ba source [17]. Figure 8 shows, a typical charge waveform of fast – timing amplifier (TA) that is likely originated near the detector surface (S) – and an event that likely occurred in the bulk (B) – each event of energy (a) 700 eV and (b) 2 keV energy, respectively, and the raw data – without cuts, are in black. The smoothed pulses in blue together with the best-fit functions (red) are also superimposed. The surface event takes over 3 μs to reach its maximum value, while the bulk event does so in about 500 ns as we can see from Figure 8. We operated dimensionally identical nGe detector as pGe detector. While for the n–type point contact germanium detector (nGe), the outer surface electrode is fabricated by boron using ion implantation technique, of submicron thickness due to which nGe has no anomalous surface effect.

The rise–time of the TA–signal (τ) is parameterized by the hyperbolic tangent function:

$$\frac{A_0}{2}\tanh(\frac{t-\tau_0}{\tau})+P_0. \qquad (1)$$

Where, A_0, P_0 and τ_0 are amplitude, pedestal offset and timing offset of the pulse.

The scatter plot of τ versus measured recoil kinetic energy (T) in keV_{ee} for events of our interest ($AC^{-}\otimes CR^{-}$) is shown in Figure 9(a, and b) for pGe and nGe detectors, respectively. For pGe, events with τ less (greater) than a selected cut–value τ_0 (= 1.23 μs) are categorized as bulk (surface) events. In contrast, nGe does not exhibit anomalous surface events, as illustrated in Figure 9 (b), where the surface event band is completely absent. The width of measured bulk and surface bands at recoiled kinetic energy (T) > 1.5 keV_{ee} is much less than the separation of bands from τ_0. The measurement of τ, therefore, provides valuable information on locations of events and efficiently differentiate surface and bulk events [3, 5]. Figure 9(a) shows behavior of distribution which is evident as two distinct bands of structures. A small fraction, about 8%, of lone events i.e., $AC^{-}\otimes CR^{-}$ events, of 3–6 keV_{ee} recoil kinetic energy region, are in the intermediate transition zone. We derived a thickness of the intermediate transition zone by studying the corresponding fractions of events with ^{241}Am (< 1 %) and ^{137}Cs (7.5 %) – sources. A thickness of 0.16 mm was derived for this zone [5]. The choice of τ_0 is equivalent to defining the spatial border line between bulk and surface event bands within this transition thickness. This gives rise to a systematic uncertainty in evaluation of pGe fiducial mass. The width of the measured bulk and surface bands at recoil kinetic energy (T) < 1.5 keV is comparable to the band separation and leads to merger of bands. Therefore, there exists contamination in bulk and surface events.

3.4 Bulk – Surface cut efficiencies measurement and correction

The calibration of bulk – surface cut requires measurement of bulk signal survival (ε_{BS}) and surface background suppression (λ_{BS}) efficiencies. These efficiencies can be obtained by relating the observed rates (B, S) and actual rates (B_0, S_0) by following the coupled equations as bellow:

$$B = \varepsilon_{BS} B_0 + (1-\lambda_{BS}) S_0, \qquad (2)$$

$$S = (1-\varepsilon_{BS}) B_0 + \lambda_{BS} S_0, \qquad (3)$$

with an additional unitarity constrain $B_0 + S_0 = B + S$. The normalization assignment (B_0, S_0) = (B, S) is made on events within τ_0 = 2.7 – 3.7 keV_{ee}. It is equivalent to setting ε_{BS} and λ_{BS} to 1.0. This energy range is selected because it is above the complications of L–shell X–rays at ~1 keV_{ee} as well as the physics region in dark matter analysis [5].

The derivation of bulk signal survival and surface background suppression efficiencies (ε_{BS}, λ_{BS}), therefore requires at least two measurements of bulk and surface events rates (B, S) where the actual rates (B_0, S_0) are known. The data taken with ^{241}Am, ^{137}Cs and in situ cosmic–ray induced fast neutrons using nGe target detector are used for obtaining bulk signal survival (ε_{BS}) and surface background suppression (λ_{BS}) efficiencies. These data sets play a complementary role in the measurement of bulk signal survival (ε_{BS}) and surface background suppression (λ_{BS}) efficiencies, as shown in Figure 10. The two allowed bands at 0.5–0.7 keV$_{ee}$ and at 2.20–2.40 keV$_{ee}$ in the inset are shown in Figure 10(a). The different orientations of the bands are consequences of different bulk to surface ratios which are due to the different penetration-depth distributions inside the detector. The surface-rich γ-events ($AC^{+}\otimes CR^{-}$) and the bulk-rich cosmic-ray induced neutron events ($AC^{-}\otimes CR^{+}$) play supplementary roles in forcing surface background suppression (λ_{BS}) and bulk signal survival (ε_{BS}) efficiencies, respectively. We can observe a common overlap region, indicating that the results are valid for the entire detector volume. It, therefore, forced us to apply these (ε_{BS}, λ_{BS}) efficiencies derived from the calibration data to the physics data pools. The energy dependence of (ε_{BS}, λ_{BS}) efficiencies are displayed in Figure 10(b). An additional data point on ε_{BS} is independently placed by comparing the measured in situ Ga-L X-ray peak at 1.3 keV$_{ee}$ after bulk and surface event selection to that predicted by the corresponding K-peak at 10.37 keV$_{ee}$. This provides a cross-check to the calibration procedures and indicates consistent results. Figure 10(b) shows that the measured ($\varepsilon_{BS,}$ λ_{BS}) are close to unity at T>1.5 keV$_{ee}$. It also shows that there is no leakage between the bulk and surface events originated away from the transition zone. The errors on (ε_{BS}, λ_{BS}) are shown in Figure 10(b). They are derived from the global fits on the allowed bands in Figure 9. Standard error propagation techniques are applied to derive the resulting uncertainties on (B_0, S_0) using following Eqns. (4) & (5).

$$B_0 = \frac{\lambda_{BS}.B - (1-\lambda_{BS}).S}{(\varepsilon_{BS} + \lambda_{BS} - 1)} \qquad (4)$$

$$S_0 = \frac{\varepsilon_{BS}.S - (1-\varepsilon_{BS}).B}{(\varepsilon_{BS} + \lambda_{BS} - 1)}. \qquad (5)$$

The uncertainties include contributions from their own measurement errors, the (ε_{BS}, λ_{BS}) calibration errors, as well as systematic uncertainties.

3.5 X – Ray Peak Study

When the cosmic ray neutrons interact with germanium nucleus, it becomes unstable germanium isotope, then decay to another nuclide via electron capture (EC), and emits an X-ray. The X-ray line at 10.37 keV$_{ee}$ arises due to the germanium

activation by both thermal and fast cosmogenic neutrons. In the thermal neutron case, the possible reaction is as follow:

$$^{70}\mathrm{Ge} + n \rightarrow {}^{71}\mathrm{Ge} \xrightarrow{EC} {}^{71}\mathrm{Ga} + \gamma(10.37 keV_{ee}), \tau_{\frac{1}{2}} = 11.4 days. \quad (6)$$

In the fast neutron case, the possible reactions are as follow:

$$^{70}\mathrm{Ge} + n \rightarrow {}^{68}\mathrm{Ge} + 3n, \quad (7)$$

$$^{68}\mathrm{Ge} \xrightarrow{EC} {}^{68}\mathrm{Ga} + \gamma(10.37 keV_{ee}) \tau_{\frac{1}{2}} = 271 days, \quad (8)$$

The intensity variation of 10.37 keV_{ee} peak with respect to time is shown in Figure 11. From Figure 11 it is clear that the intensity of 10.37 keV_{ee} peak is very high for few's days due to ^{71}Ge which half-life is around 11 days then decreasing very slowly since ^{68}Ge half-life is around 271 days and after that it becomes in equilibrium state. The fitting function used in this study is as bellow;

$$f(x) = C + A*\exp((-0.693*X)/B),$$

Where A is the fitting initial value, B is the half-life of ^{68}Ge and C is the 10.37 keV_{ee} peak activity at equilibrium state. Figure 11 reveals that data is fully explained by the above fitting function.

4. Results and discussion

4.1 Constrains on χ_N spin–independent interaction

The lone ($AC^- \otimes CR^-$) events from pGe data taken at KSNL at different stages of the analysis are shown in Figure 12(a). The solid line spectrum is of lone events having only hit in the target germanium detector (pGe). This spectrum includes both surface and bulk events. After the surface events identification and removal, the measured bulk events spectrum is plotted with dashed line and corrected bulk events spectrum is plotted with data points. One can observe that both the spectra are almost identical with improvement in energy resolution. At recoil kinetic energy (T) > 1.5 keV_{ee}, shows a direct consequence of $\varepsilon_{BS} = \lambda_{BS} = 1$. At low energy, the efficiency – correction and background – subtracting effects compensate each other in this data set. In the inset of Figure 12(a), the spectrum of the corrected surface events of the lone events ($AC^- \otimes CR^-$) data set is shown. It can be seen that no known structure is observed.

After subtracting a flat background due to high energy γ - rays and the known L-shell X-rays contributions predicted by the accurately measured K-peaks at higher energy, the residual spectrum is shown in the inset of Figure 12(b). It still shows excess of events at the sub-keV region. Their origin is not yet identified, and studies towards the understanding of these are intensely pursued. Under the conservative assumption

that WIMPs signals cannot be larger than the residual excess, constraints on χ_N cross-section ($\sigma_{\chi N}^{SI}$) versus m_χ were derived via the binned Poisson method with conventional astrophysical models [14]. The quenching function in Ge is derived with the TRIM software which matches well with existing data [14]. At a given m_χ, the flat background is measured at an energy range of at least 1.7 keV_{ee} and beyond the tail (< 1%) of the χ_N recoil spectra. They probed and excluded some of the allowed regions on light WIMPs from earlier experiments [18]. Exclusion plot of $\sigma^{SI}{}_{\chi N}$ versus m_χ at 90% confidence level is displayed in Figure 13. Bounds from other world class leading experiments are superimposed [19] for comparison. After using all the well-developed techniques summarized in above sections with 900g pGe TEXONO detector having 500 eV noise edge TEXONO experiment published his Dark Matter limits in 2013 shown in Figure 13 with red line [14].

Now we applied same techniques with our upgraded 500g pGe detector. With our upgraded 500g pGe detector we improve our noise edge from 500 eV to 300 eV [3]. Figure 14(a) shows the spectrum from RAW data, after basic filters, $AC^{-}\otimes CR^{-}$ and in inset $AC^{-}\otimes CR^{-}\otimes B$ events with 500g pGe detector. From Figure 14(a) it is clear that after applying all the well-developed techniques still in $AC^{-}\otimes CR^{-}\otimes B$ events the background is order of 10^{th}. To avoid the complication of bulk / and surface events effect we also used 500g nGe detector which have no surface anomalous effect [3] and also achieve 300 eV in noise edge shown in Figure 14(b). While by using the nGe detector we are free from surface effects, still the background level in sub-keV region is 10^{th} order as in pGe which show that sub-keV background is not only due to surface effect. Now our on-going research is to understand the excess of background in sub-keV region by optimizing our software and hard ware. We expect some new physics result soon.

4.2 Constrains on Low Energy Neutrino Physics

The physical origin and experimental consequences of finite neutrino masses and mixings are not fully understood. Investigations on anomalous neutrino properties and interactions are crucial to addressing these fundamental questions and may provide hints to the new physics beyond the Standard Model. To explore the neutrino electromagnetic properties like neutrino magnetic moments (μ_υ) [8] and neutrino milli-charge (q_υ) [11] with neutrino–electron scattering at low energy regime we need the detectors which have low threshold, low background and high energy resolution. Initially, we started studying the above mentioned physics along with neutrino – nucleus coherent scattering cross section for that we need detection threshold of 100 eV, background of the order of 1 cpkkd and detector mass of the order of 1kg. On the way to achieve the above mentioned specification we started studying the interactions of WIMP dark matter particle with the detector medium. The experimental studies on μ_υ and q_υ is making use of neutrino interactions with bound electrons of detectors. We adopted the Multi-Configuration Relativistic Random–Phase Approximation theory, to include the atomic effect in the analysis [10, 20]. It also provides better description for

the structure of Ge atoms as well as photo–absorption data of Ge crystal at photon energy ≥ 80 eV [17, 19, 20]. The differential cross-section due to q_υ has $(1/T^2)$ – dependence which is different from that of (1/T) for μ_υ at very low recoil kinetic energy i.e., (T) << E_υ, where T is the measurable recoil energy of electron and E_υ is the energy of the incoming neutrino. Figure 1(a) shows that both μ_υ and q_υ contributions are enhanced as T decreases. It was recently identified that q_υ contribution has an enhancement in cross-section when atomic effects are properly calculated and the known ratios of peaks at discrete binding energies provide smoking gun signatures for positive observations [17, 19, 20]. Figure 1(a) also reveals that the experimental sensitivity to both μ_υ and q_υ values critically depend on lowering the energy threshold of the detector employed for measurement of the recoil–electron spectrum. The expected differential event rate (dR/dT) are convoluted with the neutrino spectrum ($d\phi$ / dE_υ) as follows,

$$\frac{dR}{dT} = \rho_e \int_{E_\nu} \left[\frac{d\sigma}{dT}\right]\left[\frac{d\phi}{dE_\nu}\right] dE_\nu . \qquad (9)$$

Where, ρ_e is the electron number density per unit target mass. The observable spectra due to weak interactions, neutrino magnetic moments at $\mu_\upsilon = 2.9 \times 10^{-11}\ \mu_B$ and milli-charges at $q_\upsilon = 1.1 \times 10^{-12} e_0$, here e_0 is charge on electron, with a reactor flux of 10^{13} cm^{-2} sec^{-1} are depicted in Figure 1(a). In order to place the upper bounds on μ_υ and q_υ with the existing data, standard algorithms were adopted. Results of comparisons of different data taken with MCRRPA calculations [20] are listed in Table II. The potential sensitivities of realistic next–generation measurements with novel Ge techniques when a 1% measurement of the SM cross section could be achieved, at a threshold of 0.1 keV are also shown in last row of the Table II. Low threshold detector is also crucial in the studies of neutrino nucleus coherent scattering at the reactor [1, 2, 3]. At 100eV threshold, the range of 10 events/kg–keV–day can be expected. The observation of this channel is the current theme of the program at KSNL.

5. Conclusions

The results on efficiencies (ε_{BS}, λ_{BS}) calibration and the subsequent (B_0, S_0) measurements in pGe confirm that both signal efficiencies and background leakage to the signal region are crucial in the analysis. To overcome these difficulties, the elimination of the anomalous surface effects at the hardware raw signal level in Ge detectors is much more desirable. To these ends, the merits and operation of nGe are being studied. This detector has already proved crucial to provide calibration data to the pGe. Research efforts are being pursued to turn it into a target with comparable

sensitivities. Germanium detectors with sub–keV sensitivities have opened the windows for the studies of SM and exotic neutrino interactions as well as for the searches of light WIMPs. In particular, both pGe and nGe represent novel advances in the Ge detector techniques to cover events with sub-keV energy depositions as summarized in Table I. Continuing R & D efforts are pursued with this goal, via the optimizations of hardware configurations as well as software pulse shape discrimination techniques at sub-keV regions.

Acknowledgment

The research programs and results presented in this article are from the efforts of the TEXONO Collaboration consisting of groups from Taiwan (Academia Sinica, Kuo-Sheng Nuclear Power Station), China (Tsinghua University, Institute of Atomic Energy, Nankai University, Sichuan University), India (Banaras Hindu University) and Turkey (Middle East Technical University, Dokuz Eyll University). The authors are grateful to the contributions from all collaborators. M. K. Singh thanks to the University Grants Commission (UGC), Govt. of India, for the funding through UGC D. S. Kothari Post-Doctoral Fellowship (DSKPDF) scheme. (No. F. 4-2/2006, (BSR) /PN/15-16 10098). Authors are thankful to the Department of Science and Technology (DST), New Delhi.

References

[1] Q Yue *et al. High Energy Phys. and Nucl. Phys.* 28, 877 (2004); H T Wong *et al. J. Phys. Conf. Ser.* 39, 266 (2006); H T Wong, *Int. J. Mod. Phys.* D20, 1463 (2011).

[2] P S Barbeau, J I Collar, and O Tench, J Casual, *Astropart. Phys.* B09, 009 (2007); C E Aalseth *et al. Phys. Rev. Lett.* 101, 251301 (2008).

[3] A K Soma *et al. Nucl. Instr. Meth.* A836, 67 (2016).

[4] S Kerman *et al. Phys. Rev.* D93, 113006 (2016).

[5] H B Li *et al. Astropart. Phys.* 56, 1 (2014).

[6] C Giunti *et al. Rev. Mod. Phys.* 87, 531 (2015).

[7] H T Wong *et al. Mod. Phys. Lett.* A20 1103 (2005) and references therein.

[8] H B Li *et al. Phys. Rev. Lett.* 90, 131802 (2003); H T Wong *et al. Phys. Rev.* D75, 012001 (2007).

[9] S Davidson *et al. Phys. Lett.* B626, 151 (2005); N F Bell *et al. Phys. Lett.* B642, 377 (2006).

[10] J W Chen *et al. Phys. Lett.* B731, 159 (2014) and references therein.

[11] J W Chen *et al. Phys. Rev.* D90, 011301(R) (2014).

[12] M Drees and G Gerbier, *Review of Particle Physics Chin. Phys.* C38, 353 (2014), and references therein.

[13] H T Wong *et al. Mod. Phys. Lett.* A23 1431 (2008); S T Lin *et al. Phys. Rev.* D79, 061101(R) (2009).

[14] H B Li *et al. Phys. Rev. Lett.* 110, 261301 (2013).

[15] S K Liu *et al Phys. Rev.* D90, 032003 (2014); K J Kang *et al. Chin. Phys.* C37, 126002 (2013); W Zhao *et al. Phys. Rev.* D88, 052004 (2013); Q Yue *et al. Phys. Rev.* D90, 091701(R) (2104).

[16] P N Luke *et al. IEEE Trans. Nucl. Sci.* B36 926 (1989).

[17] E Aguayo *et al. Nucl. Instrum. Meth.* A701, 176 (2013).

[18] C E Aalseth *et al. Phys. Rev. Lett.* 106, 131301 (2011); C E Aalseth *et al. Phys. Rev. Lett.* 107, 141301 (2011).

[19] C E Aalseth *et al. Phys. Rev.* D88, 012002 (2013); C E Aalseth *et al. arXiv:*1401.3295 (2014); W Zhao *et al. Phys. Rev.* D93, 092003 (2016) and references therein.

[20] J W Chen *et al. Phys. Lett.* B731, 159 (2014); J W Chen *et al. Phys. Rev.* D91, 013005 (2015).

[21] M Deniz *et al. Phys. Rev.* D82 033004 (2010).

[22] A G Beda *et al. Adv. High Energy Phys.* 2012, 350150 (2012).

TABLE 1: Summary table of performance parameters on detector hardware and signal selection of the various Ge detectors, with data taken at KSNL [3].

Items	CoaxiGe	ULEGe	pGe	nGe	pGe
Modular Mass (g)	1000	5	900	500	500
RESET Amplitude (V)	N/A	8.0	9.8	6.8	6.8
RESET Time Interval (ms)	N/A	~700	~800	~170	~160
Pedestal Noise RMS (eV)	812	33	56	49	41
Pulser FWHM (eV)	1566	87	141	133	110
Gamma Line Width	Ga–K X–Ray	^{55}Fe	Ga–K X–Ray	Ga–K X–Ray	Ga–K X–Ray
RMS (eV)	880	64	157	104	87
Selected Trigger level Δ (σ_A)	4.3	4.3	4.2	4.2	4.2
50 % Trigger Threshold (eV)	3500	142	230	204	171
Noise-Edge (eV)	5600	230	400	373	311

TABLE 2: Summary of experimental limits at 90% CL on μ_υ and q_υ parameters studied using selected reactor neutrino data. The projected sensitivities of measurements at the specified realistically achievable experimental parameters are also shown.

Data Set	Reactor- $\bar{\upsilon}_e$ Flux 10^{13} cm^{-2} s^{-1}	Data Strength ON/OFF (kg-days)	Analysis Threshold (keV)	Bound at 90 % CL μ_υ	Bound at 90 % CL q_υ
TEXONO CsI(Tl) [21]	0.64	29882.0/7369.0	3000	< 22.0	< 170.0
TEXONO 1 kg HPGe [8]	0.64	570.7/127.8	12	< 7.4	< 8.8
GEMMA ~1.5 kg HPGe [22]	2.7	1133.4/280.4	2.8	< 2.9	< 1.1
TEXONO nGe [11]	0.64	124.2/70.3	0.3	< 26.0	< 2.1
Projected [11,3]	2.7	800/200	0.1	< 1.7	< 0.06
Sensitivity at 1% of SM [11, 3]	1.0	--------	0.1	< 0.023	< 0.0004

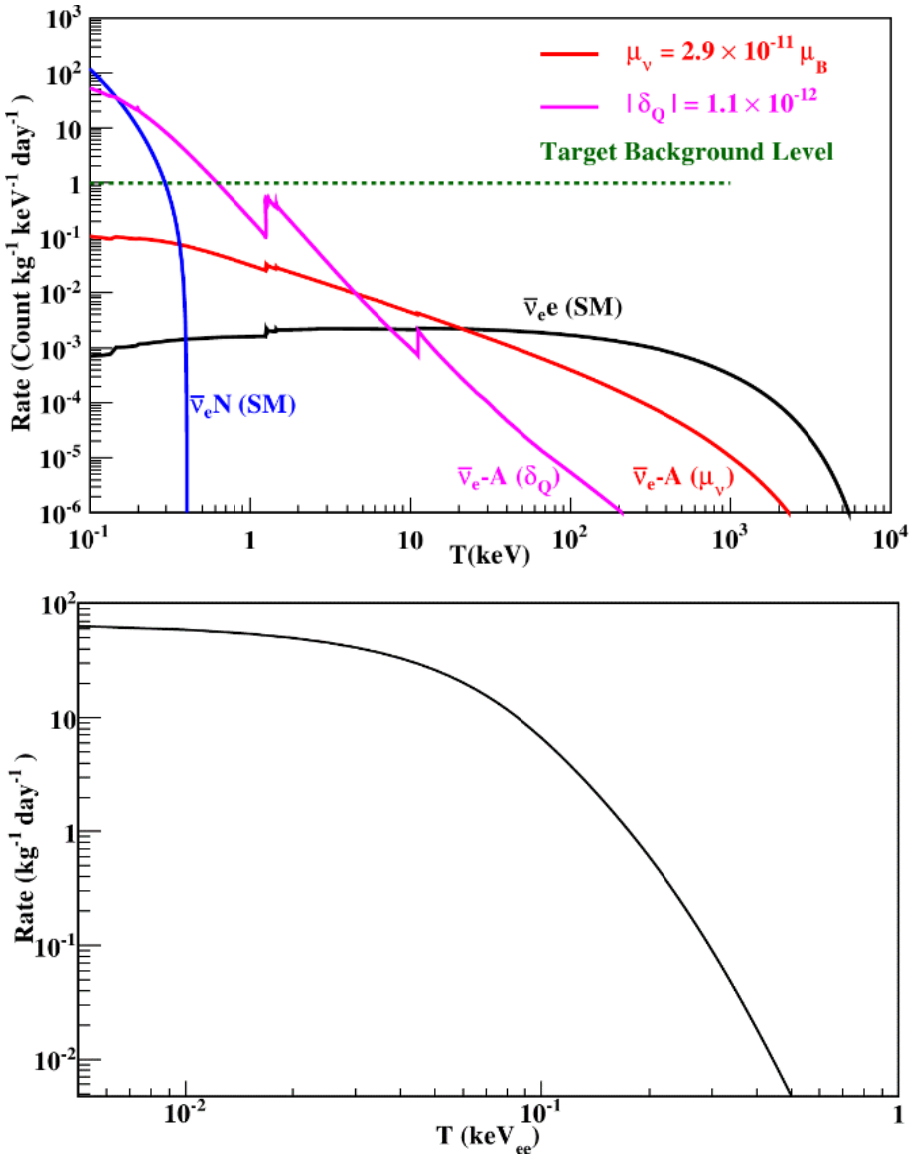

FIGURE 1: (a) The observable spectra due to reactor – $\bar{\upsilon}_e$ interactions on Ge target with ϕ ($\bar{\upsilon}_e$) = 10^{13}cm^{-2} s^{-1}, neutrino magnetic moment and neutrino milli-charge fraction at the current bounds from direct experimental searches: $\mu_\upsilon = 2.9 \times 10^{-11}\ \mu_B$ and $|\delta_Q| = 1.1 \times 10^{-12}$, respectively. Overlaid are the SM $\bar{\upsilon}_e$–e and coherent scattering $\bar{\upsilon}_e$–N. Quenching effects of nuclear recoils are taken into account. The target background level of 1 kg^{-1} keV^{-1} day^{-1} is marked. (b) Expected integral $\bar{\upsilon}_e$–N coherent scattering rates due to SM contributions at the same flux, as a function of physics threshold, assuming realistic detector resolution.

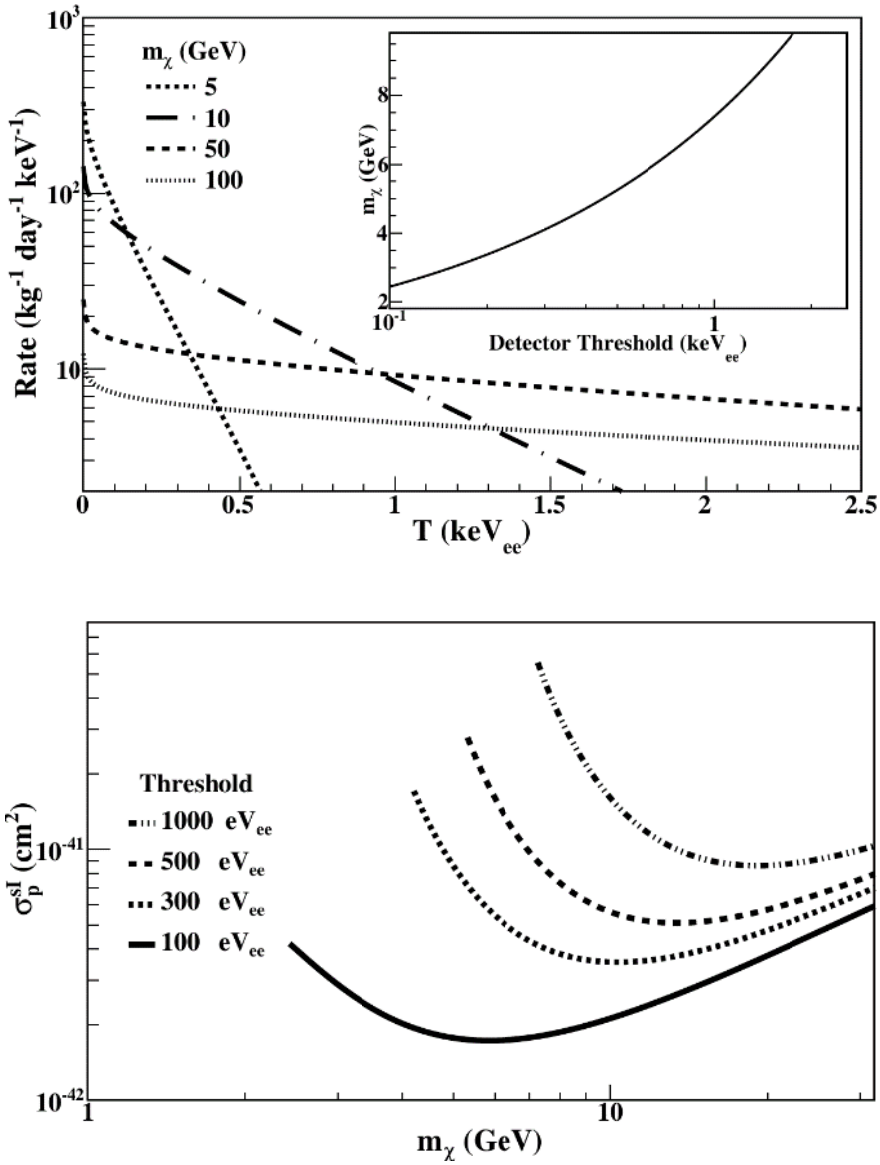

FIGURE 2: (a) Measurable recoil spectra for WIMP-Ge interactions at a cross-section of 10^{-40} cm^2, at various values of m_χ. The lower bounds of m_χ as a function of physics threshold is shown in the inset, assuming 1 kg–yr of data and a background level of 1 kg^{-1}keV^{-1}day^{-1}. Quenching effects of nuclear recoils are taken into account. (b) Sensitivity reaches of the same configuration at different detector threshold, showing the relative improvement in cross–section as a function of m_χ.

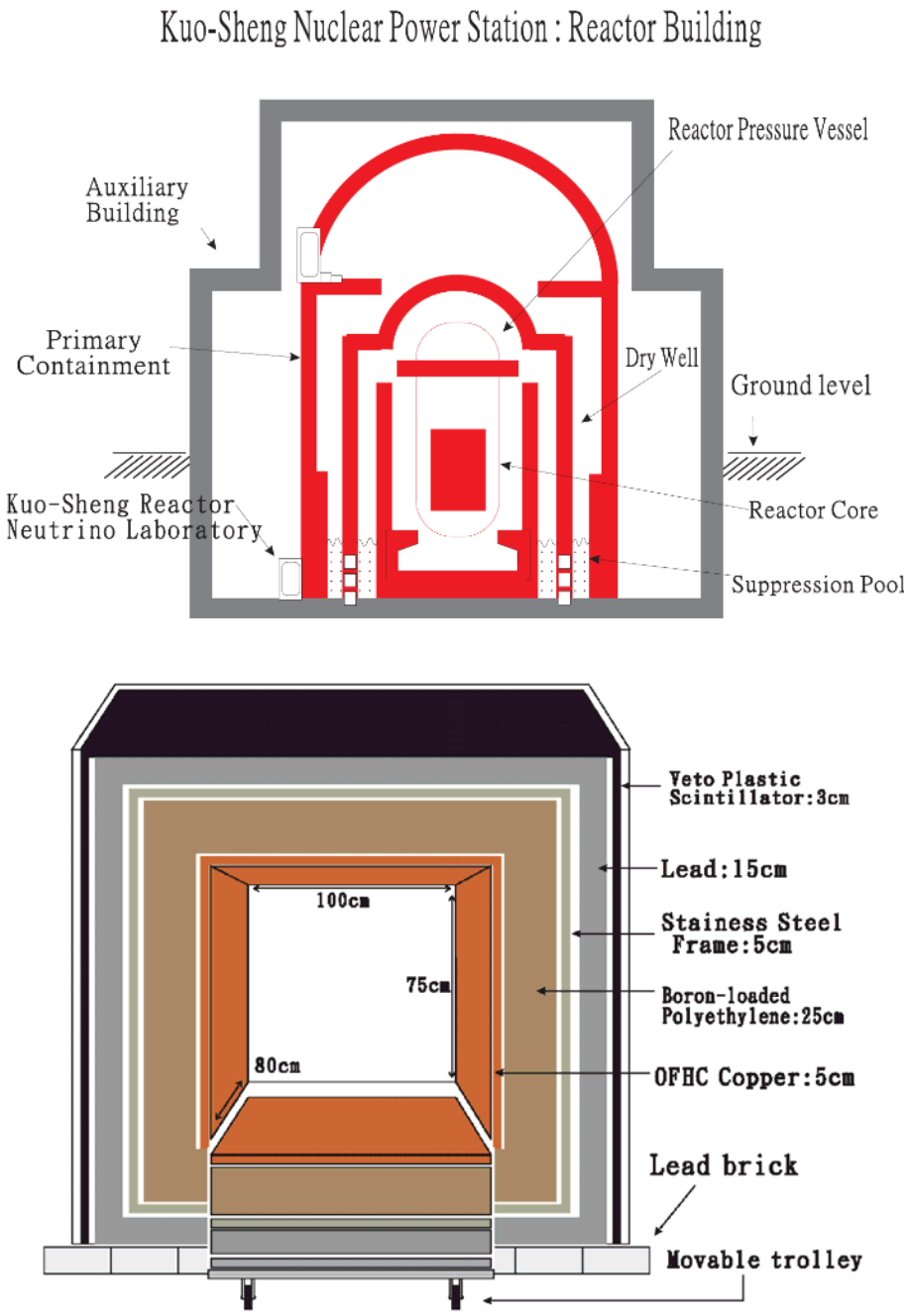

FIGURE 3: (a) Schematic side view, not drawn to scale, of the Kuo-Sheng Nuclear Power Station Reactor Building, indicating the experimental site. (b) Schematic layout of the general purpose inner target space, passive shielding and cosmic ray veto panels.

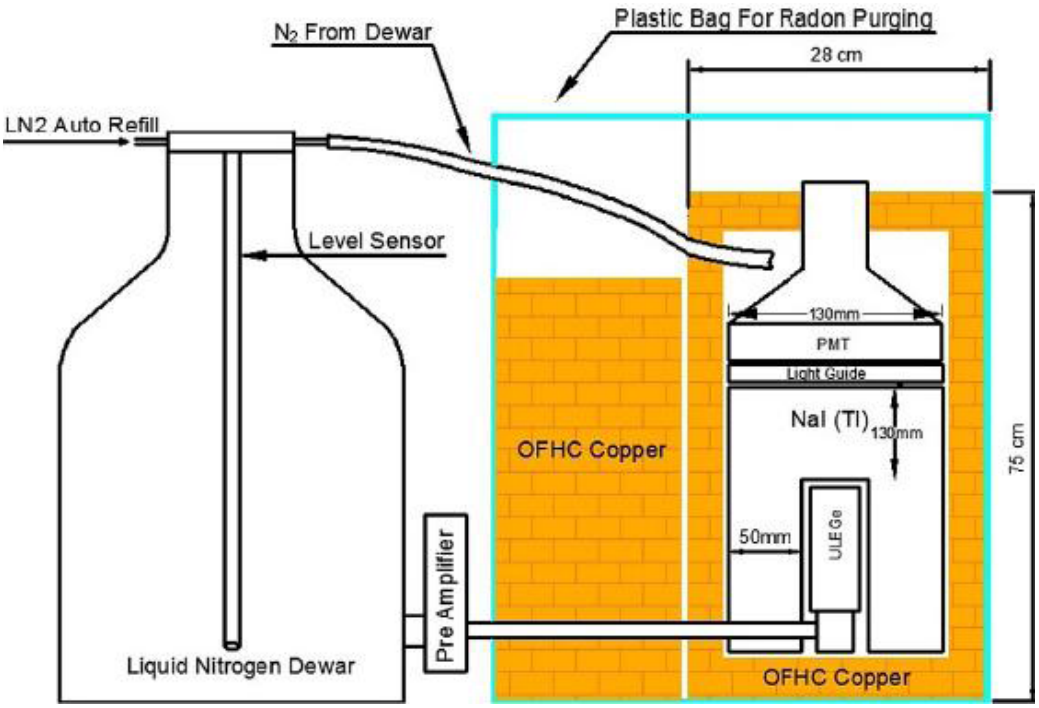

FIGURE 4: Schematic diagram of the experimental set-up which includes the Ge and NaI(Tl) scintillator. The hardware is placed inside a 50 ton shielding structure, surrounded by plastic scintillators as cosmic–ray vetos.

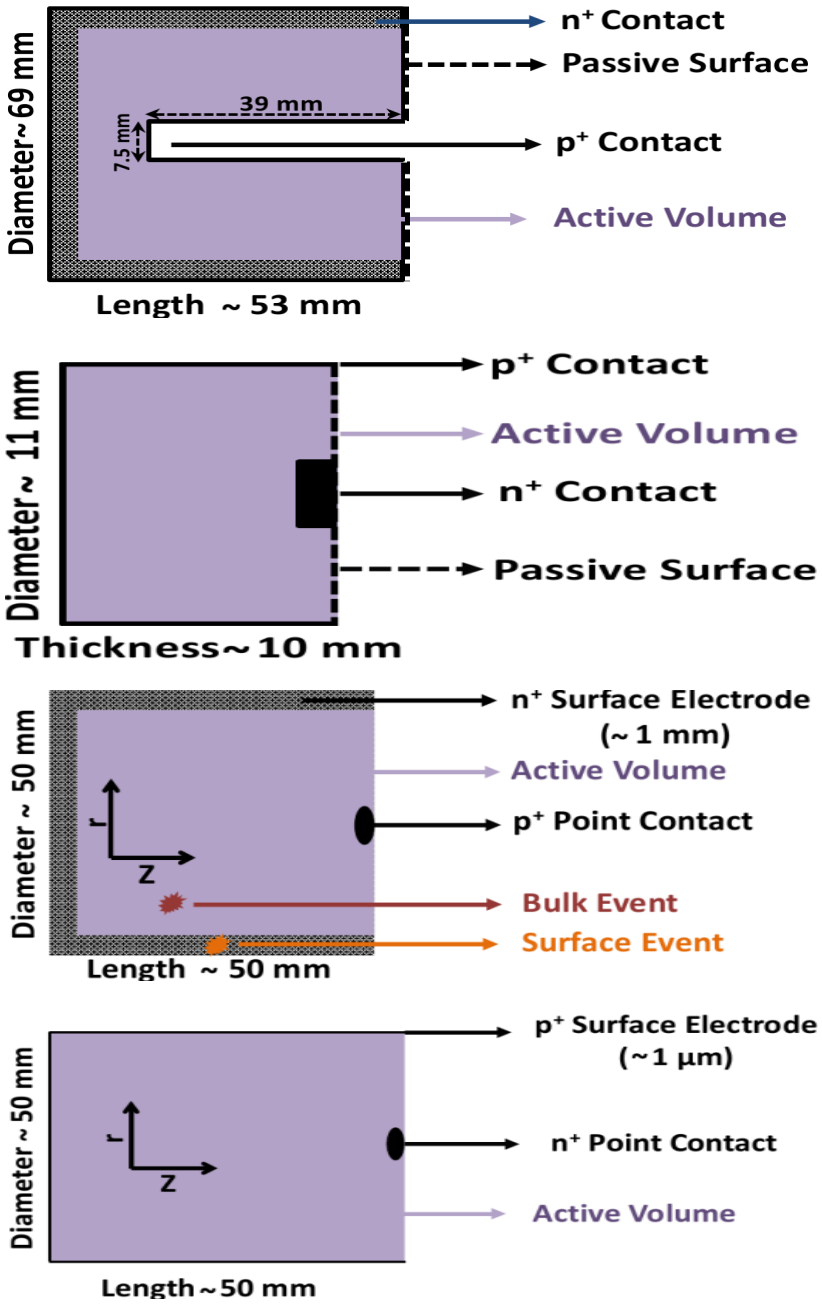

FIGURE 5: Schematic crystal configurations of the Ge detectors: (a) coaxial HPGe at 1 kg mass (b) ULEGe at 5 g modular mass (c) pGe at 900 g mass and (d) nGe at 500 g mass.

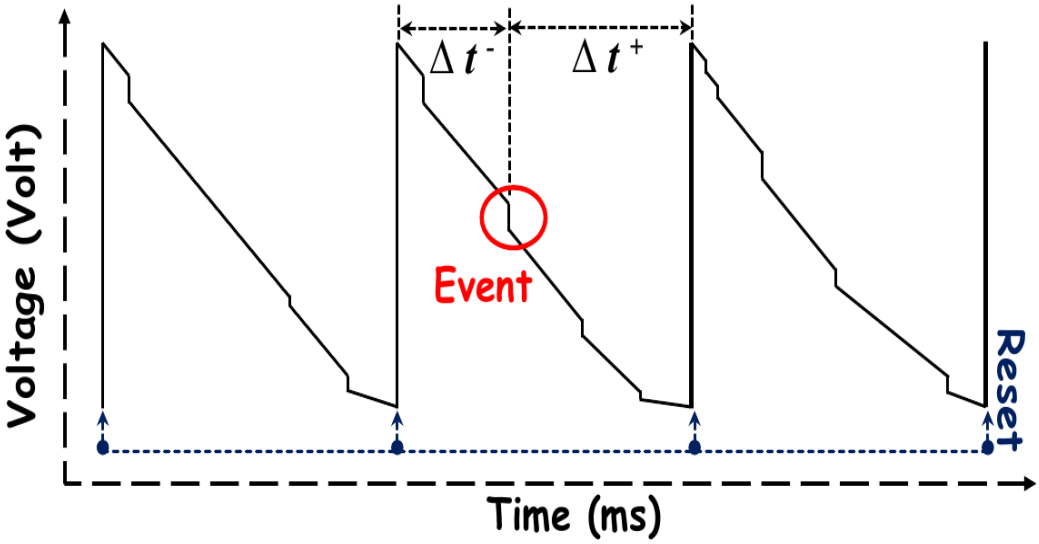

(a)

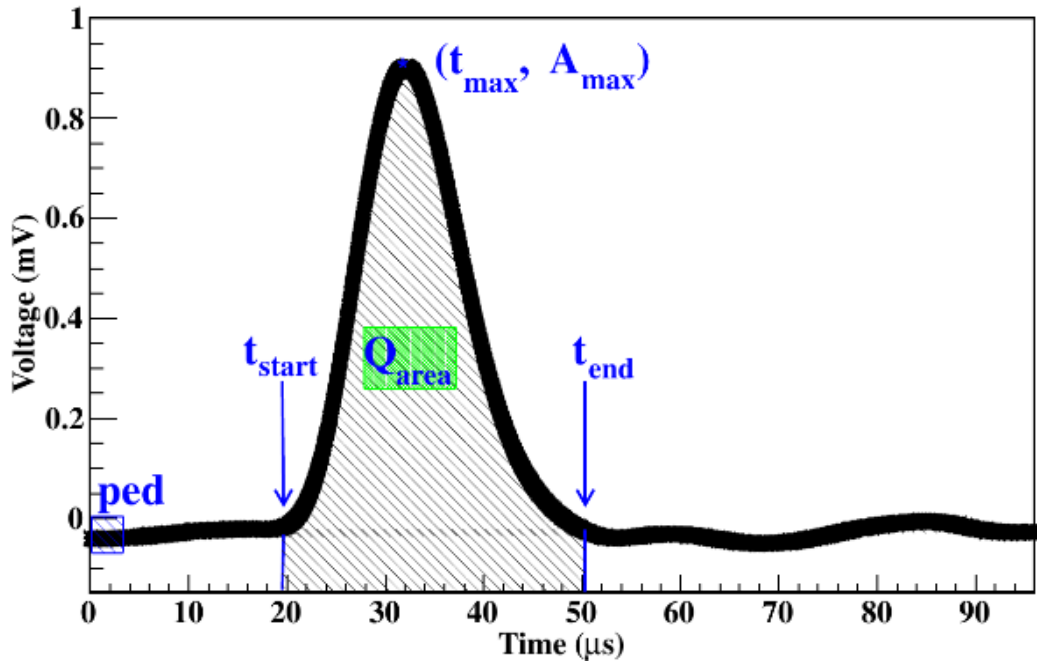

(b)

FIGURE 6: (a) Schematic drawing of the raw preamplifier signals as recorded with oscilloscope. (b) Shaping amplifier (Canberra 2026) output with definitions of some of the analysis parameters.

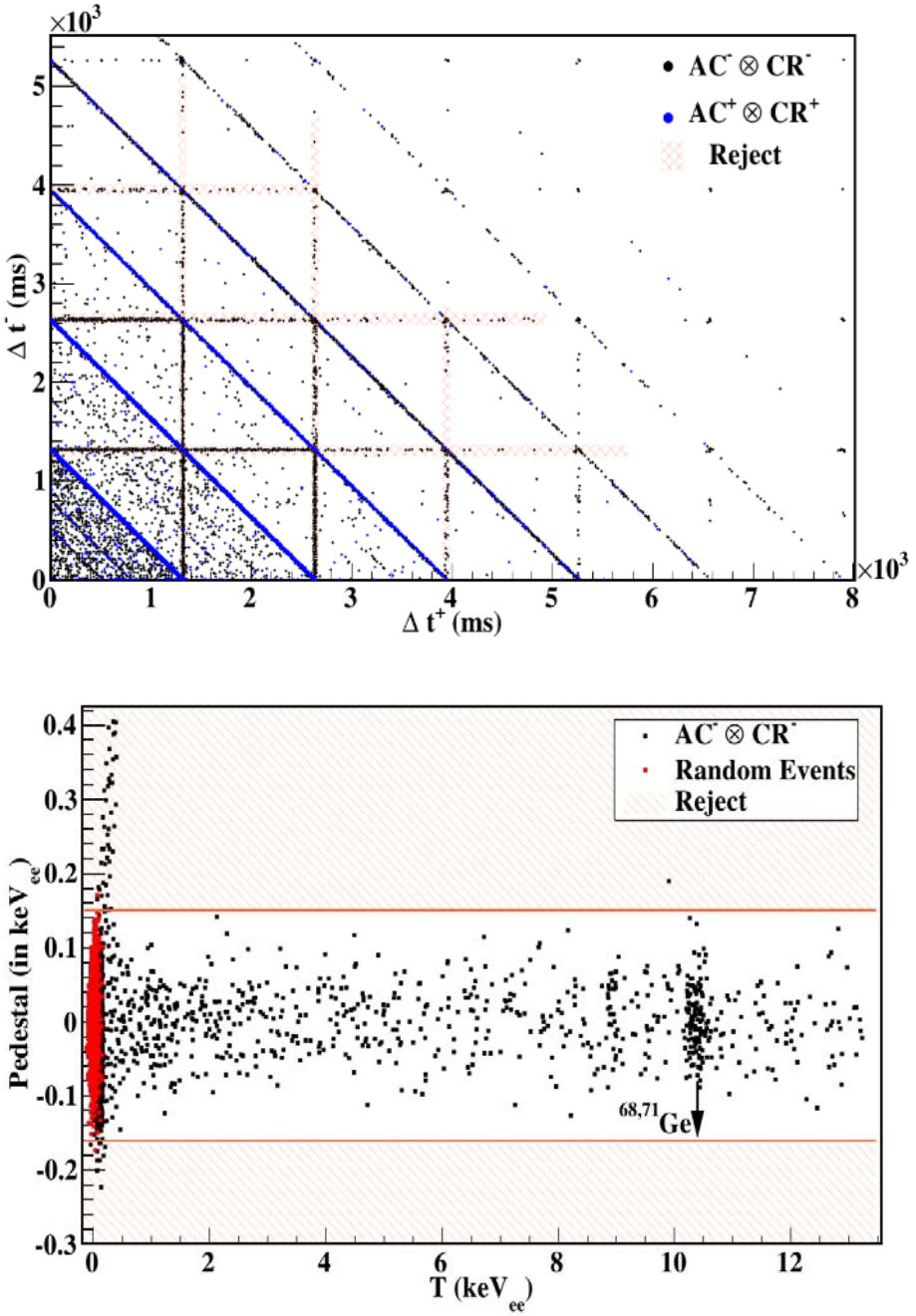

FIGURE 7: (a) Events timing with respect to reset signal, where Δt^+ and Δt^- are correspondingly the next and previous reset signal. (b) Events selection based on fluctuation of pedestal.

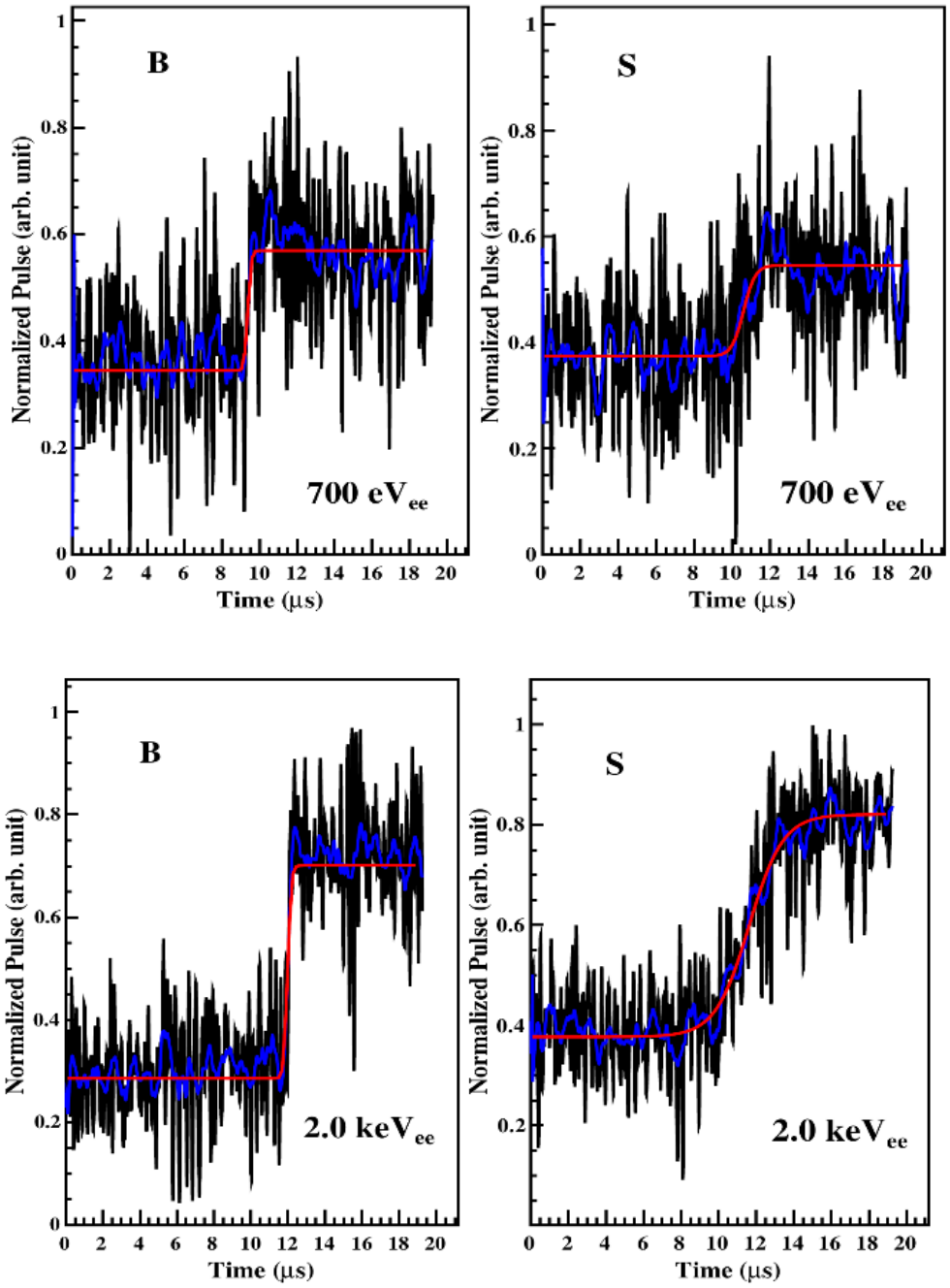

FIGURE 8: (a) Typical S/B events at (a) 700 eV and (b) 2 keV energy with raw pulses shown in black. The smoothed (blue) pulses, together with the best-fit functions (red) are also superimposed.

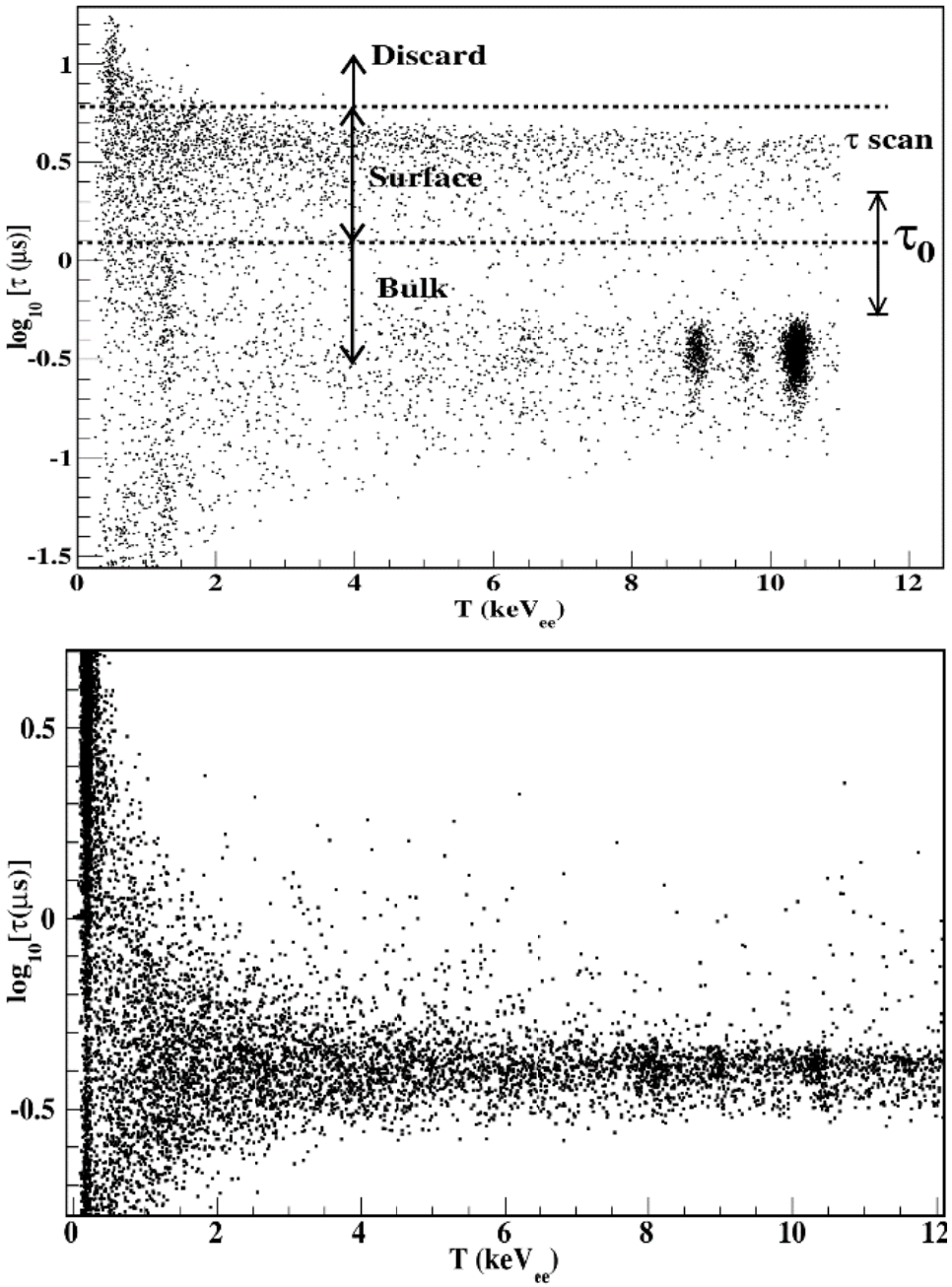

FIGURE 9: (a) pGe τ distribution at low background configuration. τ_0 defines the surface-bulk selection criteria. (b) nGe τ distribution at low background configuration and demonstrates the absence of anomalous surface events.

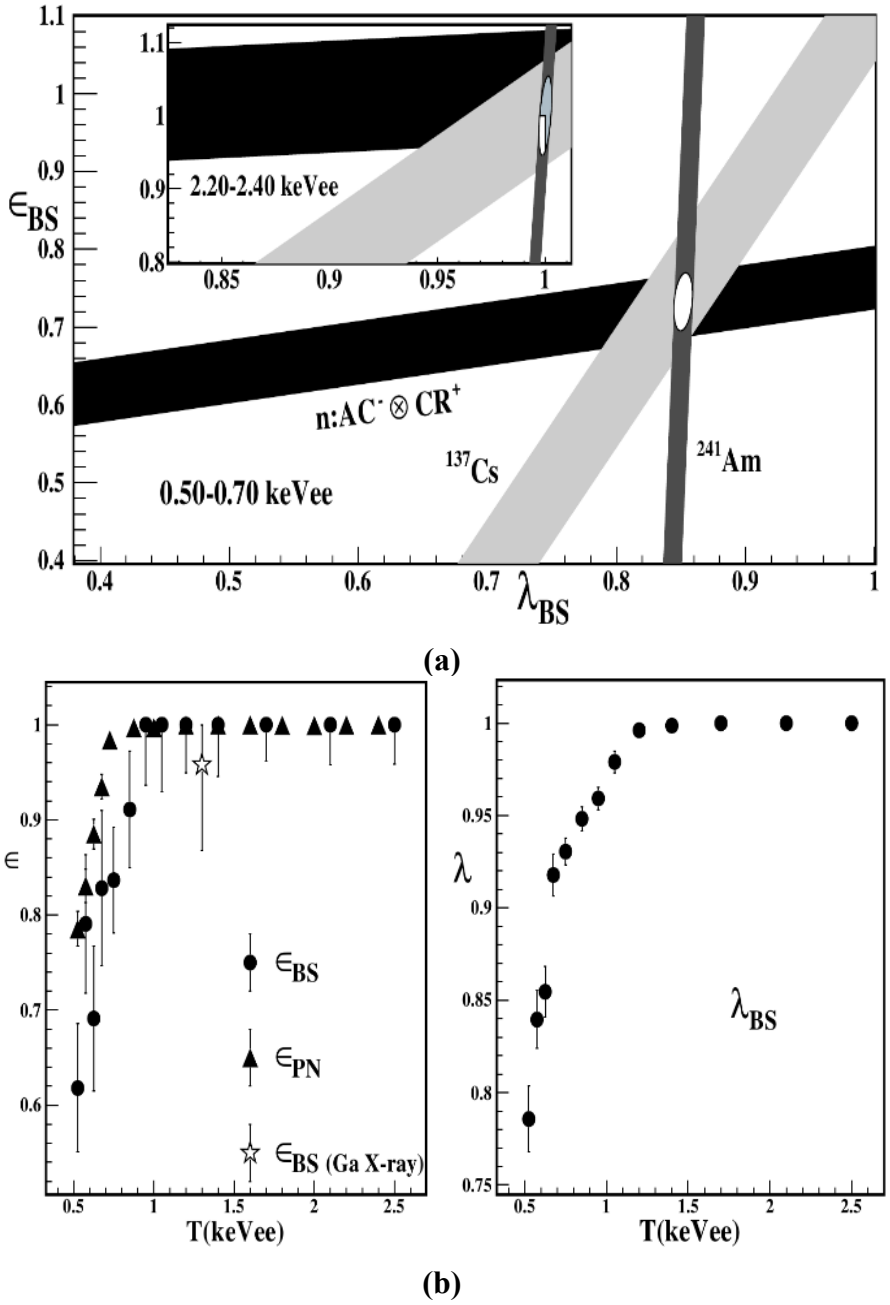

FIGURE 10: (a) Allowed bands at threshold and at a high energy band. (b) The measured (ε_{BS}, λ_{BS}) and ε_{PN} as functions of energy. Independent measurement on ε_{BS} with Ga–L X – rays is included.

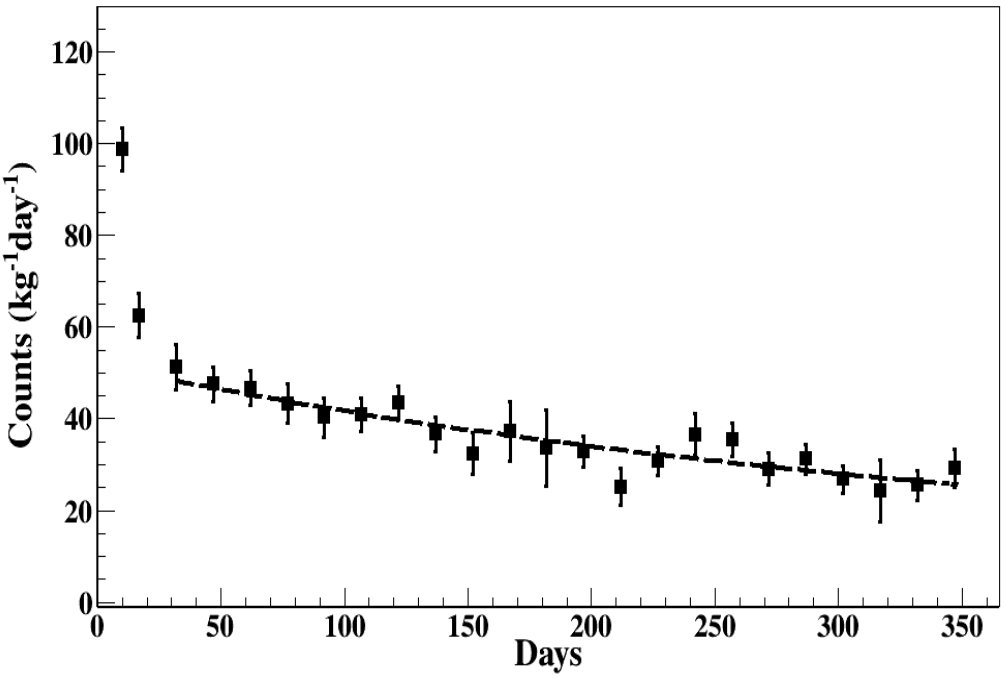

FIGURE 11: Intensity variation of 10.37 keV (X-Ray) peak with respect to time.

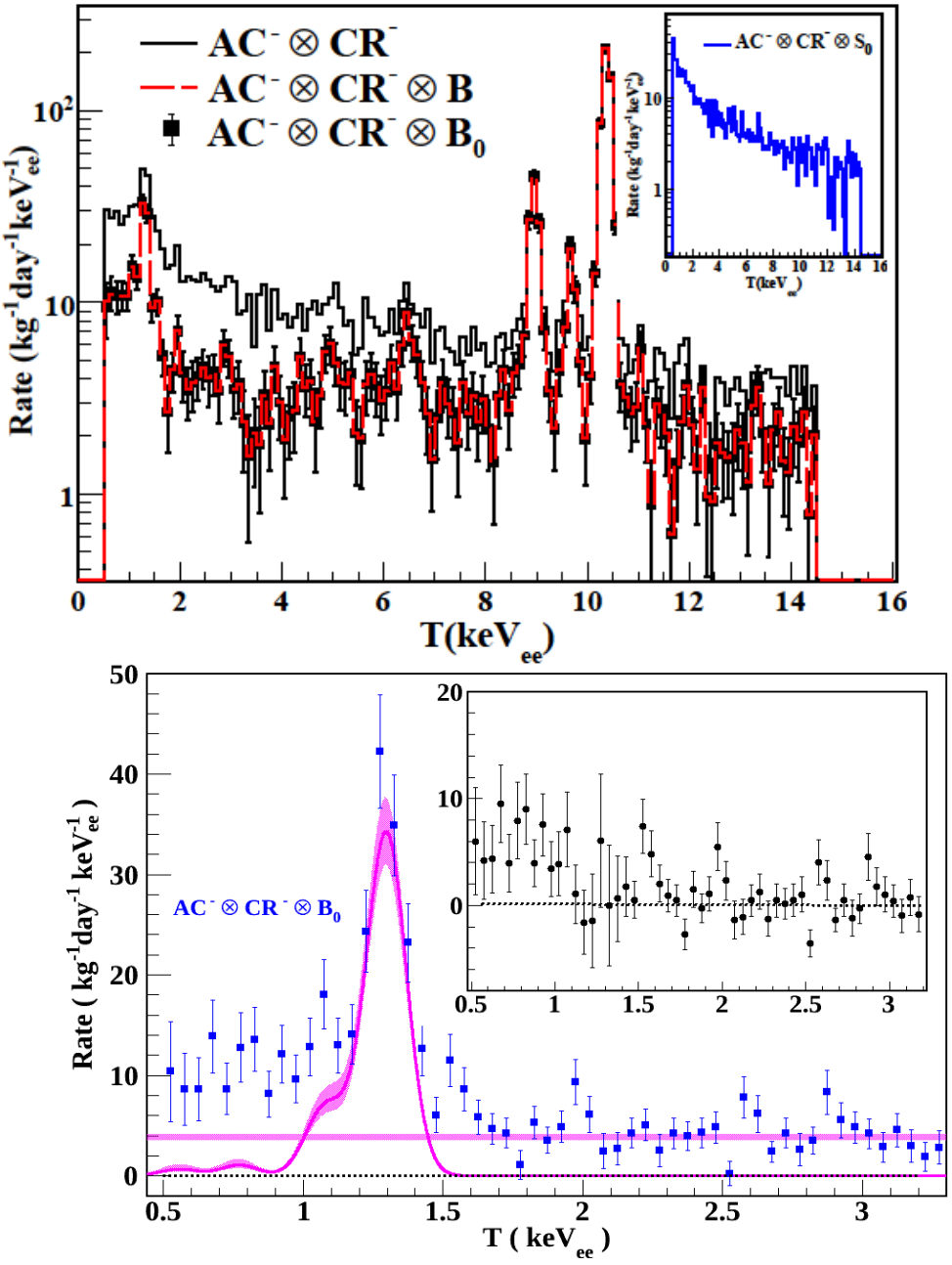

FIGURE 12: (a) Measured and corrected spectra of the $AC^{-}\otimes CR^{-}$ tag. (b) Shown in magenta are flat background due to high – energy γ – rays from ambient radioactivity, and contributions from the L – shell X-rays. The inset depicts the residual spectrum after background subtraction.

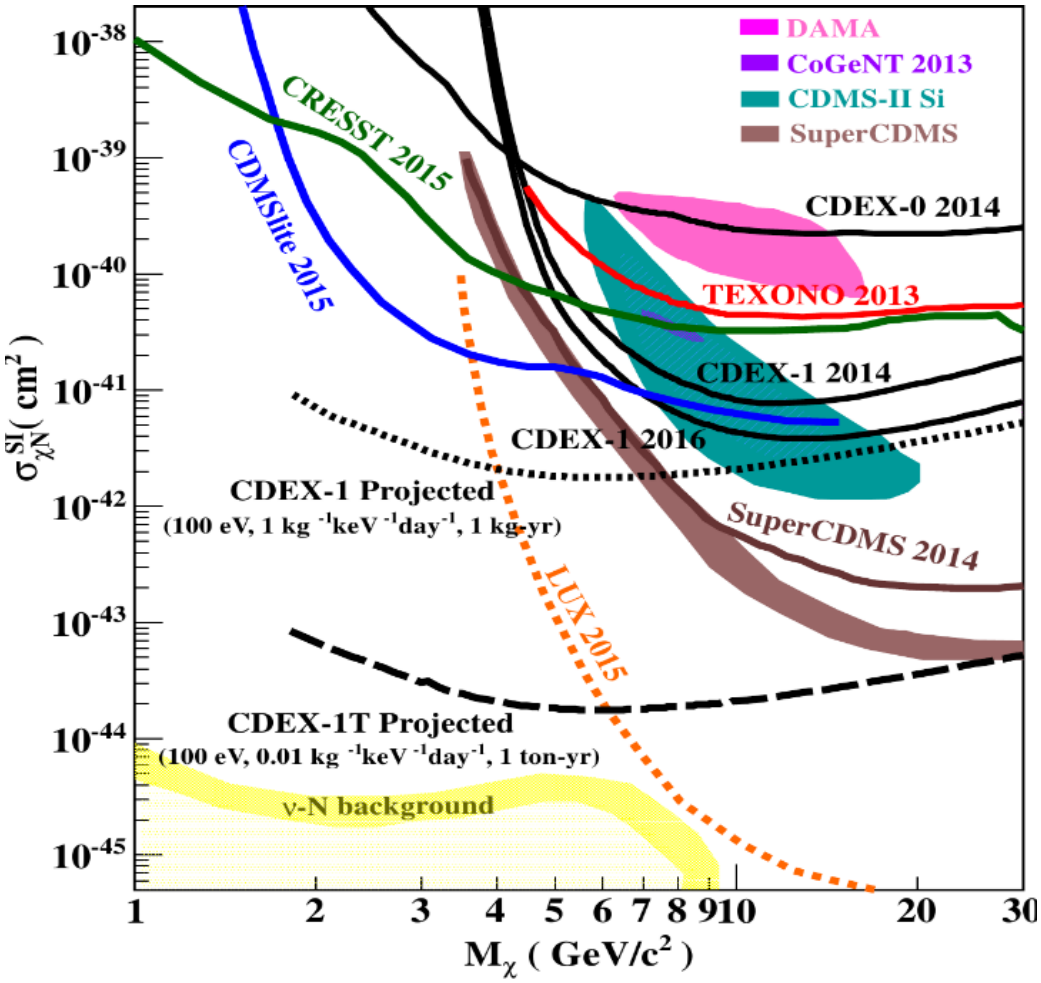

FIGURE 13: Exclusion plot of spin-independent χ_N coupling at 90% confidence level, superimposed with the results from other benchmark experiments.

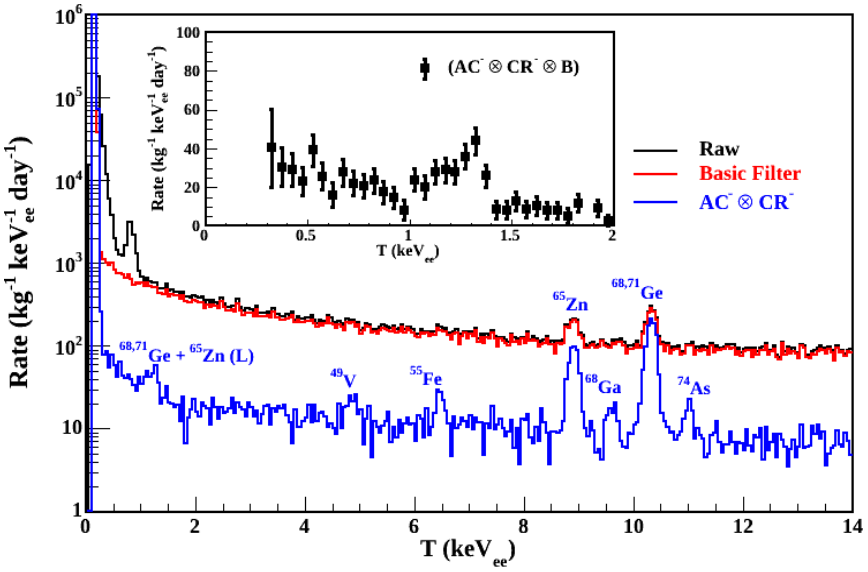

(a)

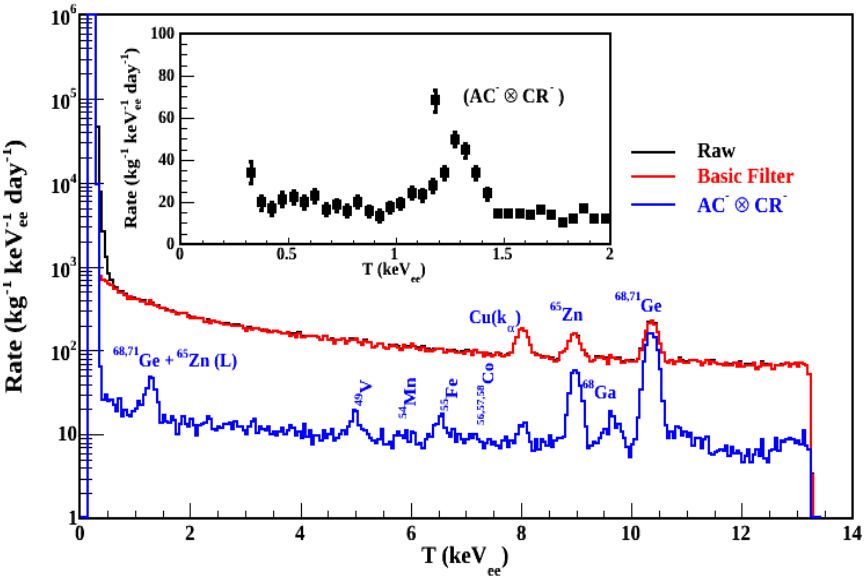

(b)

Figure 14: Evolution of AC⁻⊗CR⁻ spectra taken with the (a) pGe detector and (b) nGe detector at KSNL, from RAW data via basic filters, AC and CR vetoes, and the BS - selection for pGe detector.